Supplemental Material to:

The contrasting surges of North and South Chongtar Glacier in the central Karakoram

Frank Paul[1], Livia Piermattei[2], Desiree Treichler[2], Lin Gilbert[3], Andreas Kääb[2], Ludivine Libert[4], Thomas Nagler[4], Tazio Strozzi[5], Jan Wuite[4]

Supplemental Tables

Table S1: Overview of the Landsat (and two Sentine-2) satellite images used for delineating glacier extents and determination of frontal advance rates. All scenes have been downloaded from earthexplorer.usgs.gov. The 'Date' format is DD MM YY without leading zero's. The scenes that have been selected for each glacier (might differ due to local clouds) are marked in the last three columns (x: yes, –: no). Glacier names: 'N.-Ch.': North Chongtar, 'S.-Ch.': South Chongtar.

Nr.	Satellite	Sensor	Path	Row	Date	NN9	N.-Ch.	S.-Ch.
1	Landsat 1	MSS	159	35	24 2 73	–	x	–
2	Landsat 3	MSS	160	35	19 8 79	–	x	–
3	Landsat 5	TM	148	35	17 11 89	–	x	–
4	Landsat 5	TM	148	35	19 8 91	–	x	–
5	Landsat 5	TM	148	35	7 7 93	–	x	–
6	Landsat 5	TM	148	35	7 9 98	x	x	–
7	Landsat 7	ETM+	148	35	4 9 00	x	x	–
8	Landsat 7	ETM+	148	35	9 8 02	x	x	–
9	Landsat 7	ETM+	148	35	14 8 04	x	x	–
10	Landsat 7	ETM+	148	35	12 8 09	x	x	–
11	Landsat 5	TM	148	35	10 8 11	–	x	–
12	Landsat 8	OLI	148	35	30 7 13	x	x	–
13	Landsat 8	OLI	148	35	1 7 14	–	x	–
14	Landsat 8	OLI	148	35	4 7 15	x	x	–
15	Landsat 8	OLI	148	35	24 9 16	–	x	–
16	Landsat 8	OLI	148	35	29 10 17	x	x	–
17	Landsat 8	OLI	148	35	29 8 18	x	x	–
18	Landsat 8	OLI	148	35	31 7 19	–	x	–
19	Landsat 8	OLI	148	35	4 11 19	x	–	–
20	Landsat 8	OLI	148	35	6 12 19	–	x	–
21	Landsat 8	OLI	148	35	12 4 20	x	–	–
22	Landsat 8	OLI	148	35	28 4 20	–	–	x
23	Landsat 8	OLI	148	35	30 5 20	–	x	–
24	Landsat 8	OLI	148	35	2 8 20	–	x	x
25	Landsat 8	OLI	148	35	19 9 20	x	–	x
26	Landsat 8	OLI	148	35	5 10 20	–	–	x
27	Landsat 8	OLI	148	35	21 10 20	–	x	x
28	Landsat 8	OLI	148	35	6 11 20	x	–	x
29	Landsat 8	OLI	148	35	10 2 21	x	x	x
30	Landsat 8	OLI	148	35	1 5 21	x	x	x
31	Sentinel-2	MSI	43	SFV	6 6 21	x	–	x
32	Sentinel-2	MSI	43	SFV	16 7 21	x	–	x
33	Landsat 8	OLI	148	35	5 8 21	x	–	-

Table S2: Overview of the Landsat 7 (L7), Landsat 8 (L8), TerraSAR-X (TSX), Sentinel-2 (S2) and Planet (PL) satellite image pairs used for flow velocity analysis. The table is also listing for each scene pair the stable terrain velocities (mean and standard deviation 'std') and the observed maximum flow velocities for the three glaciers NN9, North Chongtar 'N Ch.' and South Chongtar 'S Ch.'.

					Stable terrain		Maximum velocity flowline		
	Sensor	**Start date (YYYY/MM/D)**	**End date (YYYY/MM/D)**	**Time interval (days)**	**Mean (m d^{-1})**	**Std (m d^{-1})**	**NN09 (m d^{-1})**	**N Ch. (m d^{-1})**	**S Ch. (m d^{-1})**
1	L7	2000/09/04	2002/08/04	699	0.01	0.03	0.30	0.14	0.14
2	L8	2013/07/30	2014/07/01	336	0.05	0.11	0.62	0.63	0.23
3	L8	2014/07/01	2015/07/04	368	0.04	0.14	0.76	0.54	0.23
4	L8	2015/07/04	2016/09/24	448	0.07	0.14	0.50	0.53	0.25
5	L8	2016/09/24	2017/10/29	400	0.03	0.07	0.42	0.45	0.36
6	L8	2018/07/12	2019/07/31	384	0.02	0.06	0.75	0.46	0.40
7	TSX	2011/11/12	2011/12/04	22	0.01	0.01	0.10	0.35	0.24
8	TSX	2012/09/09	2012/11/25	77	0.01	0.01	0.11	0.36	0.27
9	TSX	2014/04/10	2014/05/24	44	0.01	0.01	0.08	0.24	0.25
10	S2	2016/11/14	2017/11/04	355	0.04	0.02	0.22	0.27	0.30
11	S2	2107/07/27	2018/08/06	375	0.02	0.02	0.24	0.28	0.31
12	S2	2018/08/06	2019/08/06	365	0.03	0.03	0.35	0.30	0.40
13	S2	2019/08/06	2019/09/25	50	0.08	0.06	0.48	0.90	0.91
14	S2	2019/09/25	2020/08/25	335	0.02	0.03	0.44	0.90	-
15	S2	2020/08/25	2020/10/09	45	0.18	0.06	0.83	1.05	-
16	S2	2019/09/25	2020/06/21	270	0.09	0.19	-	-	1.15
17	S2	2020/06/21	2020/07/11	20	0.32	0.37	-	-	4.38
18	S2	2020/07/11	2020/08/25	45	0.30	1.12	-	-	16.62
19	S2	2020/08/25	2020/08/30	5	1.64	1.37	-	-	25.68
20	S2	2020/08/30	2020/09/19	20	0.23	1.27	-	-	26.77
21	S2	2020/09/19	2020/09/24	5	1.72	1.69	-	-	25.32
22	S2	2020/09/24	2020/10/04	10	0.67	1.65	-	-	24.52
23	S2	2020/10/04	2020/10/09	5	1.27	0.98	-	-	26.25
24	S2	2020/10/09	2020/10/19	10	0.42	0.59	-	-	24.05
25	S2	2020/10/19	2020/11/03	15	0.70	1.09	-	-	16.64
26	S2	2020/11/03	2020/11/08	5	1.17	0.94	-	-	14.85
27	S2	2020/11/08	2020/12/03	25	1.35	2.44	-	-	12.30
28	S2	2020/12/03	2020/12/18	15	0.23	0.31	-	-	10.00
29	S2	2020/12/18	2021/01/02	15	0.32	0.15	-	-	9.49
30	S2	2021/01/02	2021/01/12	10	0.68	0.37	-	-	8.54
31	S2	2021/01/12	2021/01/27	15	0.34	0.25	-	-	8.87
32	S2	2021/01/27	2021/02/16	20	0.30	0.59	-	-	8.13
33	S2	2021/02/16	2021/04/27	70	0.45	1.06	-	-	6.70
34	S2	2021/04/27	2021/05/02	8	1.63	0.30	-	-	8.17
35	PL	2020/06/23	2020/06/30	7	0.50	0.53	-	-	4.62
36	PL	2020/06/30	2020/07/04	4	1.19	1.05	-	-	5.51
37	PL	2020/07/04	2020/07/14	10	0.81	0.97	-	-	5.48
38	PL	2020/07/14	2020/07/20	6	2.73	2.72	-	-	8.43
39	PL	2020/07/20	2020/07/30	10	7.32	5.30	-	-	13.89
40	PL	2020/07/30	2020/08/08	9	0.71	1.59	-	-	17.79
41	PL	2020/08/08	2020/08/16	8	0.44	0.69	-	-	15.15
42	PL	2020/08/16	2020/08/24	8	0.62	0.69	-	-	22.20
43	PL	2020/08/24	2020/09/01	8	2.95	5.14	-	-	23.32
44	PL	2020/10/05	2020/10/08	3	2.01	1.81	-	-	30.81
45	PL	2020/10/08	2020/10/11	3	2.35	2.69	-	-	26.87
46	PL	2020/10/11	2020/10/15	4	1.32	3.86	-	-	27.99
47	PL	2020/10/15	2020/10/18	3	1.30	2.94	-	-	26.13

Table S3: Co-registration accuracy analysis over selected stable terrain areas (off-glacier, slope <40°). 'Std.' is standard deviation.

Datasets	Mean	Std.	Median	Minimum	Maximum
HMA DEM 2015 – SPOT 2010 (30 m)	1.3234	9.8660	1.0303	-104.01	379.3369
HMA DEM 2015 – SPOT 2015 (30 m)	0.5066	13.2438	-0.1199	-51.09	423.1772
HMA DEM 2015 – SRTM 2000 (30 m)	0.6316	9.3655	1.0229	-113.01	154.4829
SPOT 2020 – HMA DEM 2015 (5 m)	1.2817	3.0735	1.0840	-176.69	61.5708
SPOT 2010 – SRTM 2000 (30 m)	*-0.5831*	*11.4501*	*-0.3081*	*-365.42*	*143.2505*
SPOT 2015 – SPOT 2010 (30 m)	*0.7842*	*15.8529*	*1.2217*	*-424.44*	*118.0737*
SPOT 2020 – SRTM 2000 (30 m)	*2.3728*	*8.7969*	*2.5359*	*-103.09*	*59.3291*
SPOT 2020 – SRTM 2000 (5 m)	*3.0963*	*11.0475*	*3.4722*	*-257.99*	*101.4824*

Supplemental Figures

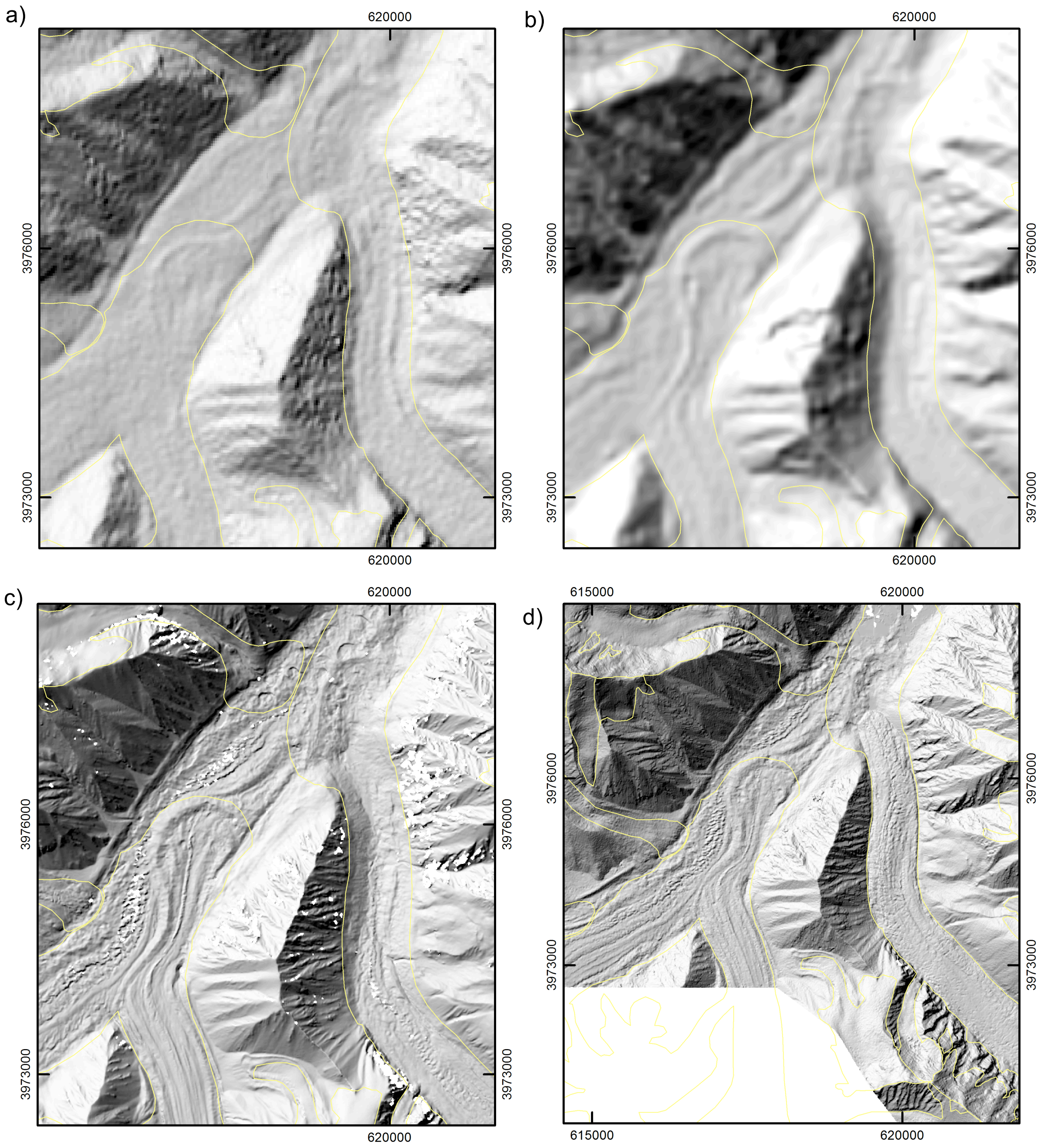

Fig. S1: Comparison of hillshades of the DEMs used. a) SRTM DEM (30 m, Feb. 2000), b) SPOT DEM (40 m, 2010), c) HMA DEM (8 m, 16.07.2017), d) SPOT Pleiades (3 m, 20.10.2020). The SPOT 2015 DEM (not shown) has the same visual/accuracy properties as the SPOT 2010 DEM shown here. Coordinates: UTM 34N [m].

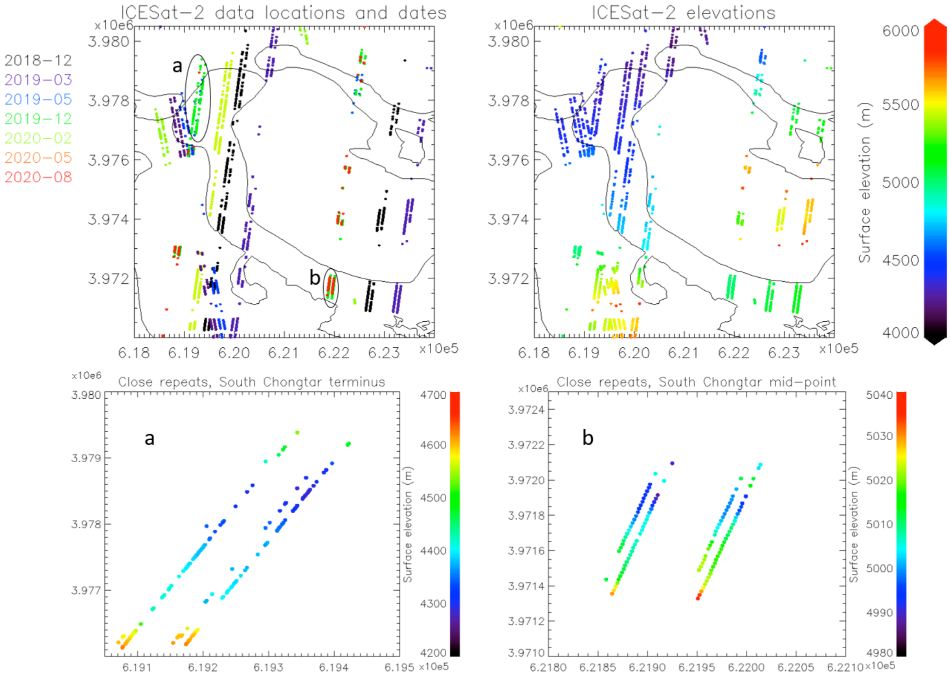

Fig. S2: ICESat-2 ATL06 data locations, coloured by date (in years and months, above left) and elevation (in m, above right). Elevations for closely repeating tracks in the two ringed areas a and b are shown below on a larger scale, demonstrating their separation.

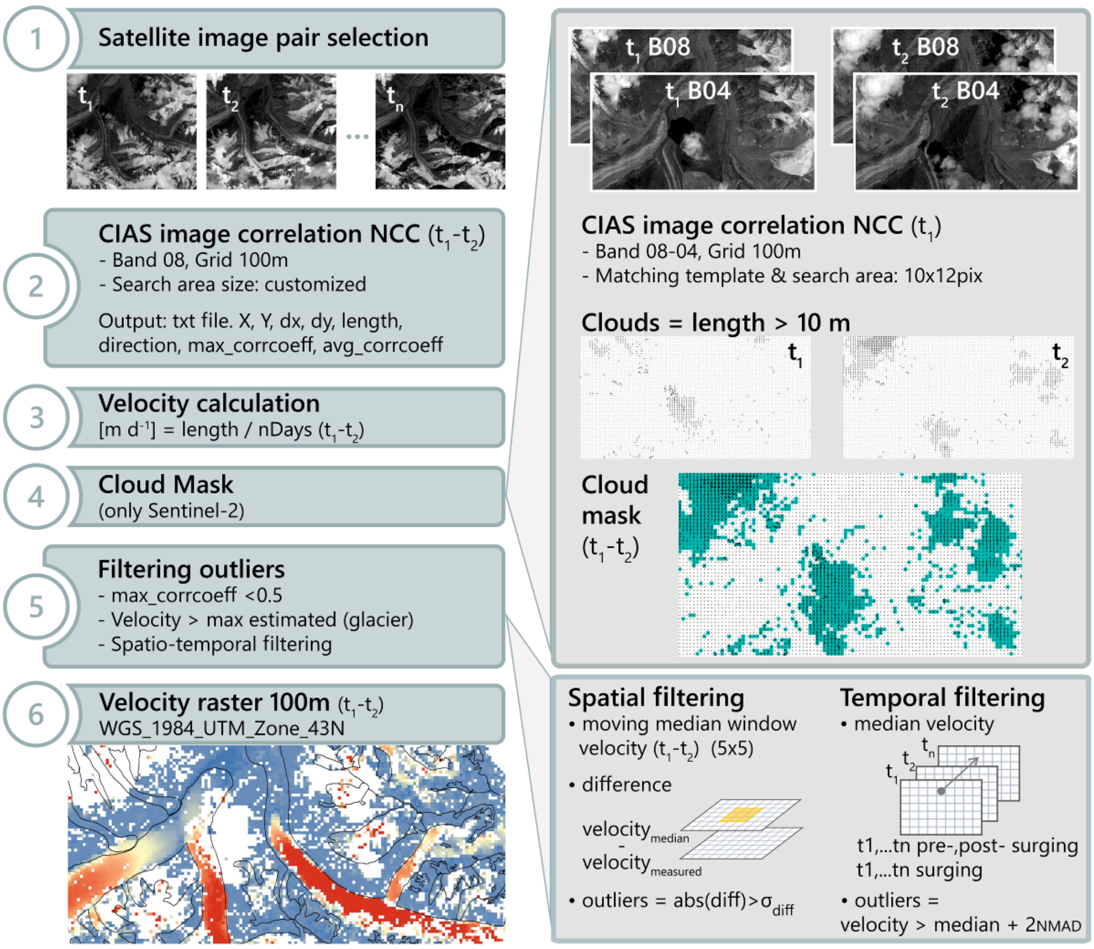

Fig S3: Workflow to calculate glacier surface displacement with CIAS.

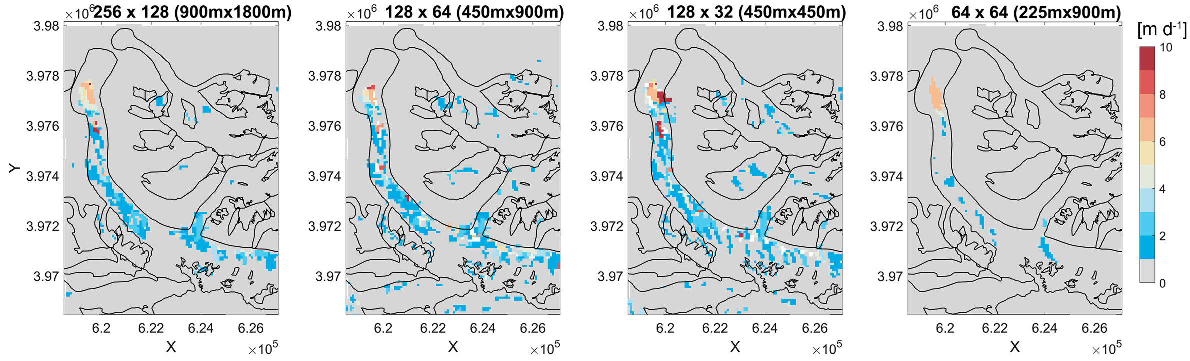

Fig. S4: Sentinel-1 image template size tests (extensions are given on top of each panel).

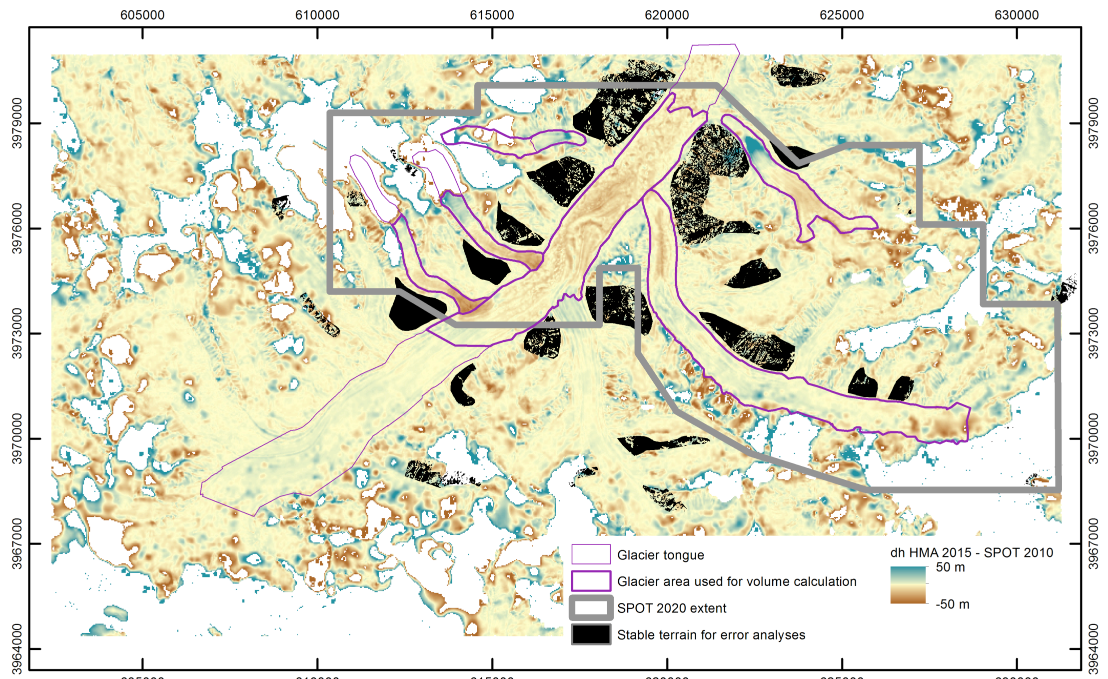

Fig. S5: Stable areas, error assessment and volume changes: Several patches of stable terrain with slope < 40° (black regions) were used to co-register the DEMs and to estimate uncertainties for both elevation changes and velocity analyses. Surge volume changes were computed for the purple glacier tongue parts, specifically adjusted from the maximum glacier outlines shown in Figs. 1 and 3, to capture the area of maximum volume changes for each glacier separately, and to remove no data/biased accumulation areas. In the background: elevation differences between HMA DEM 2015 – SPOT 2010, which are very similar to the SPOT 2015 – SPOT 2010 in Fig. 11b.

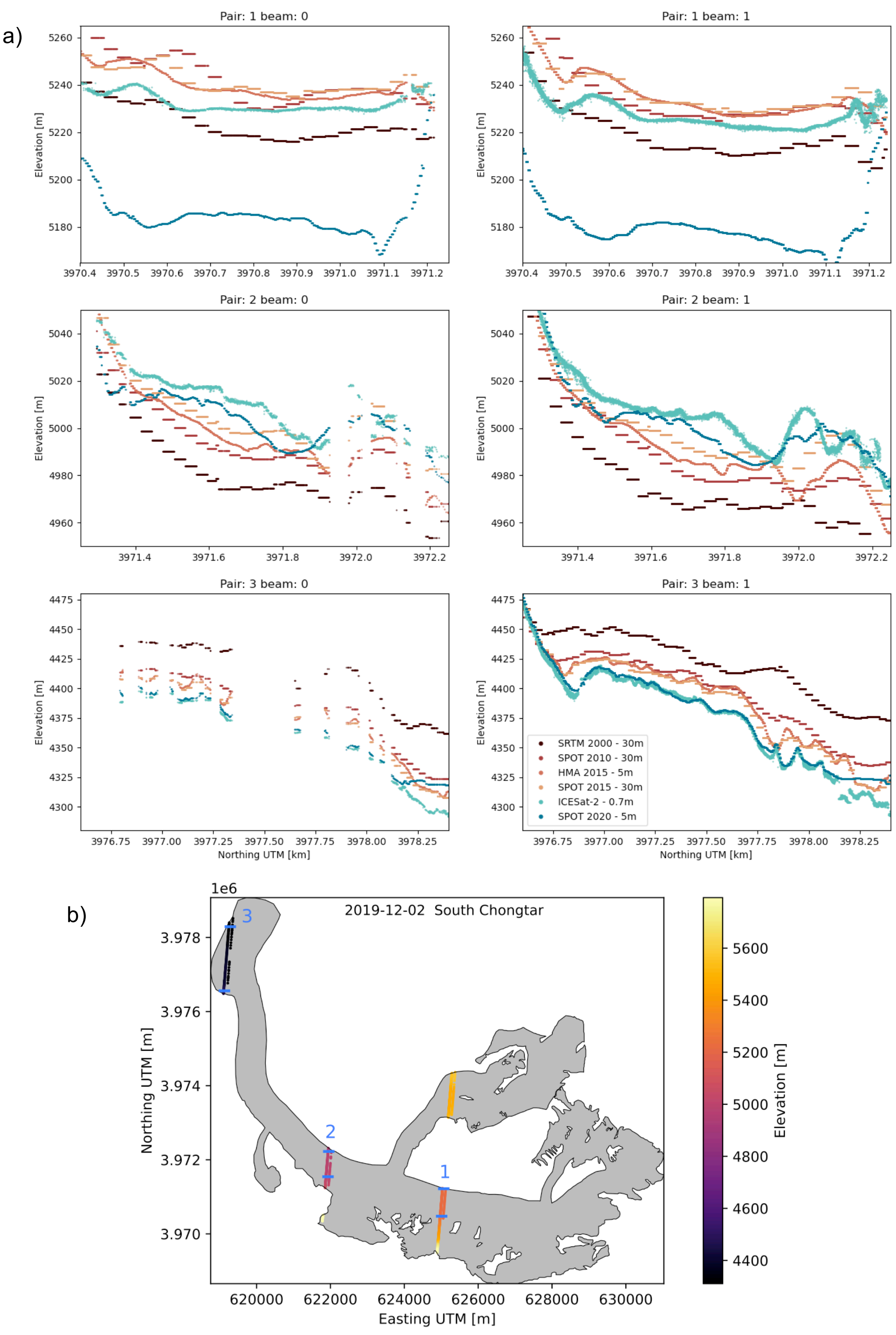

Fig. S6: a) Elevation profiles of one ICESat-2 overpass over the tongue of South Chongtar glacier on 2 February 2019. Filtered ATL03 photon elevations are shown in blue, corresponding SRTM DEM elevations in black. The profiles are numbered from East to West (see map in panel b), i.e. profile 1 is highest up on the glacier. The left panels show the weak laser beam, the right panels the strong laser beam with ca. four times as many photons per pulse shot. b) Locations of the six elevation profiles on South Chongtar glacier in a). The blue markers and numbers indicate which part of the glacier tongue is shown in a), and the profile number. The easternmost beam of each pair is the weak beam.

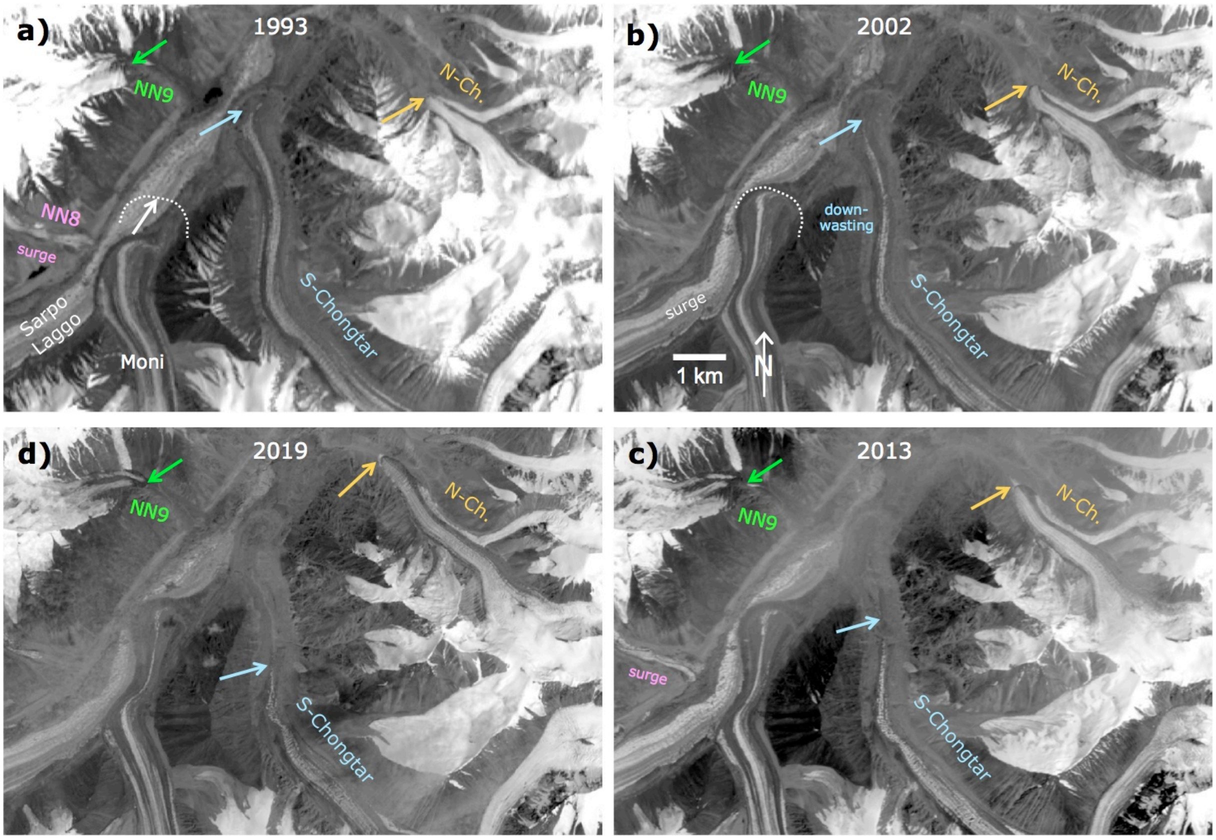

Fig. S7: Time series of glacier extents before the surge of South Chongtar (S. Chongtar) as seen with (clockwise) a) Landsat 5 in 1993, b) Landsat 7 in 2002, c) Landsat 8 in 2013 and d) Landsat 8 in 2019. The arrows at each glacier point to the terminus position at the time of image acquisition. The two surges of the neighbouring glacier NN8 are also indicated, N-Ch. is North Chongtar. The advance of North Chongtar and the downwasting of South Chongtar can be well followed. The advance of NN9 is limited. (Image source: earthexplorer.usgs.gov).

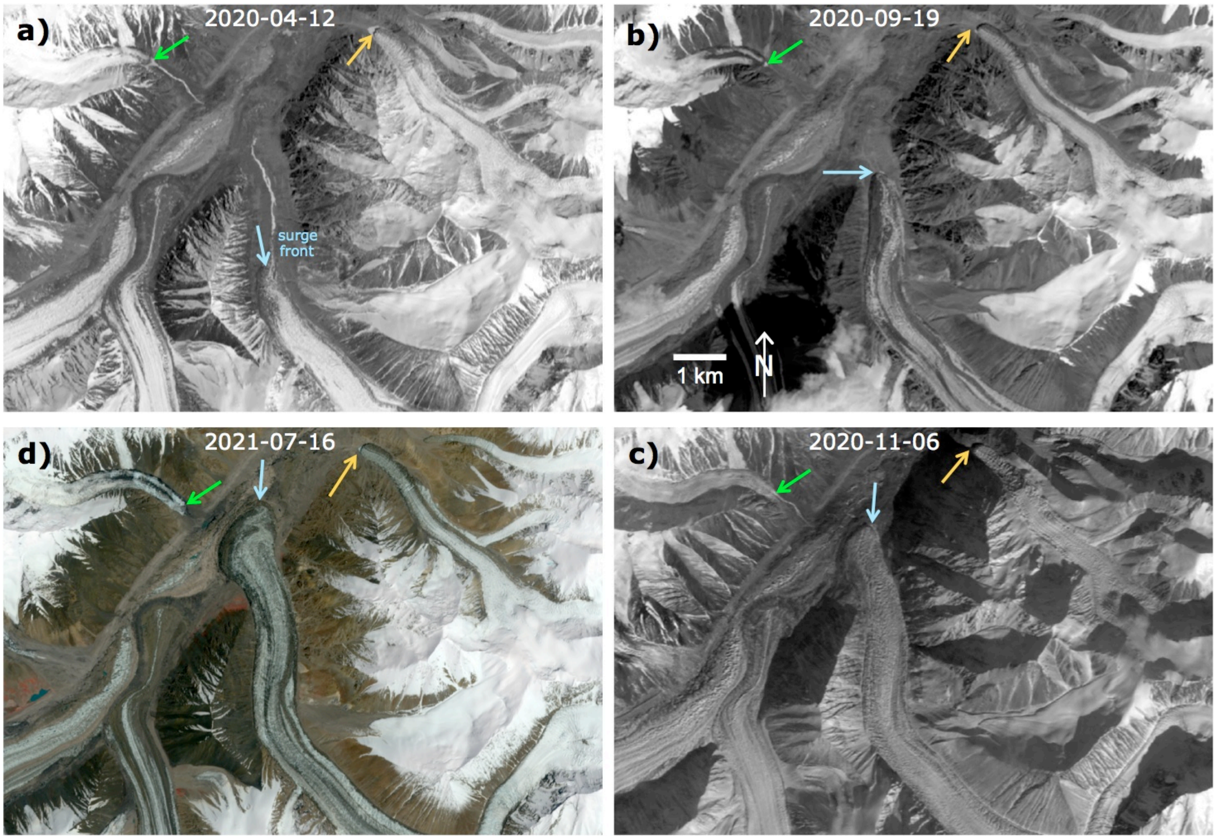

Fig. S8: Time series of glacier extents during the surge of South Chongtar (S. Chongtar) as seen with the Landsat 8 panchromatic band (clockwise) in a) 12 April 2020, b) 19 September 2020, c) 6 November 2020 and d) with Sentinel-2 on 17 June 2021. The arrows at each glacier point to the terminus position at the time of image acquisition. (Image sources: earthexplorer.usgs.gov (Landsat 8), Copernicus Sentinel data 2021).

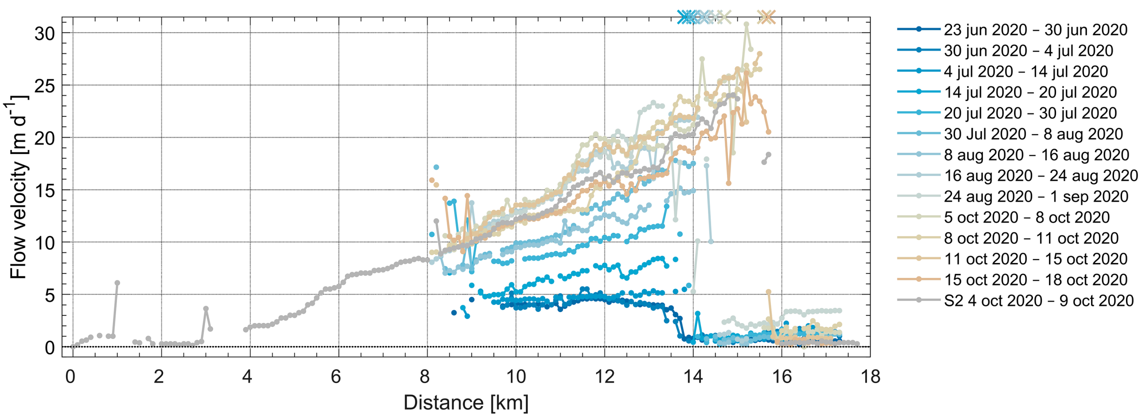

Fig. S9: Flow velocity time series derived from Planet (surge phase South Chongtar). The 'x' letters at the top mark the terminus position.

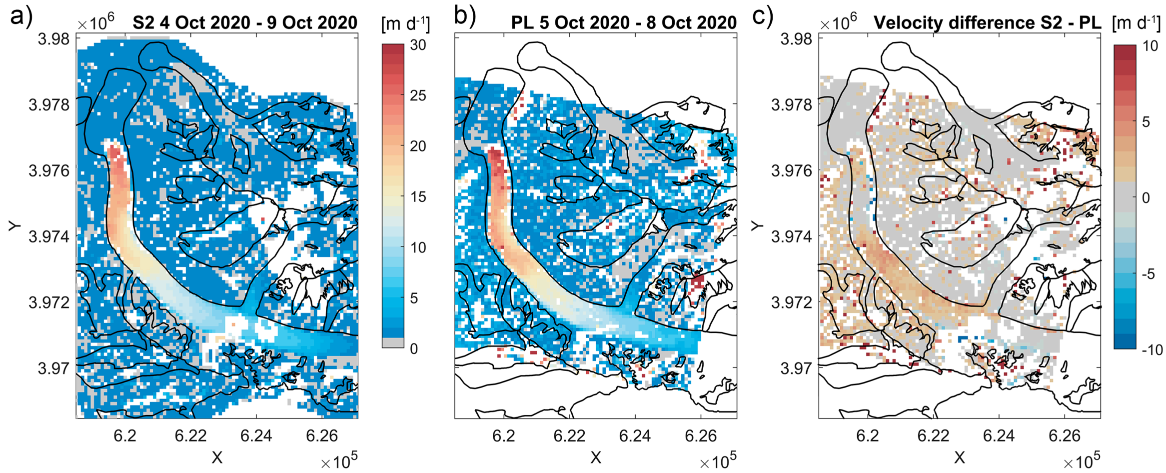

Fig. S10: 2D flow velocity maps. Comparison between a) Sentinel-2, b) Planet, and c) their difference.

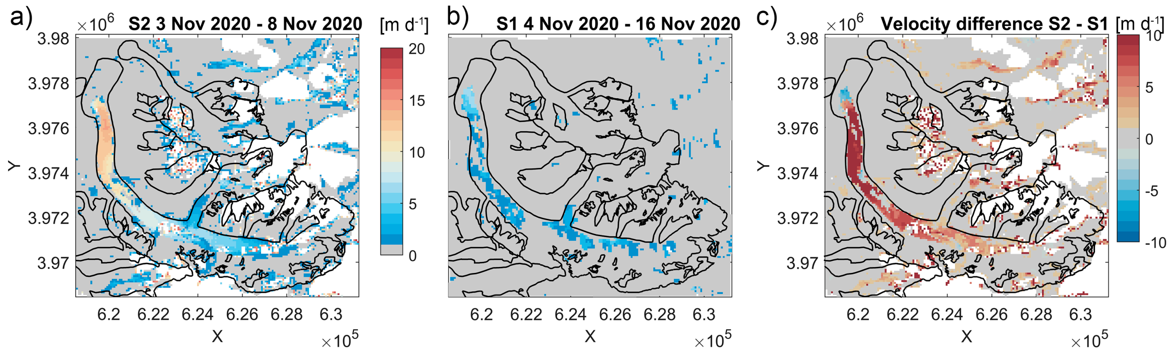

Fig. S11: 2D flow velocity maps. Comparison between a) Sentinel-2, b) Sentinel-1, and c) their difference.

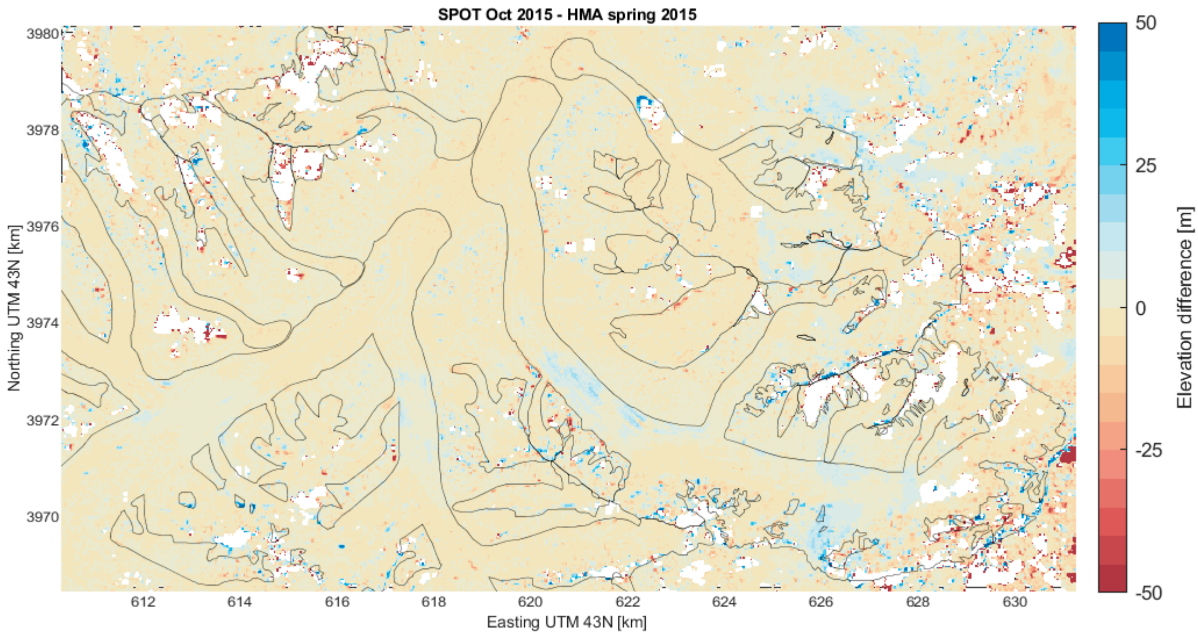

Fig. S12: DEM comparison subtracting the SPOT 2015 from the HMA 2015 DEM. It is likely that the negative values (red colours) to the east of 625 000 m E are a tiling artefact in the HMA DEM, caused by elevation source data from 2010 which contributes to the composite in this part of the DEM.

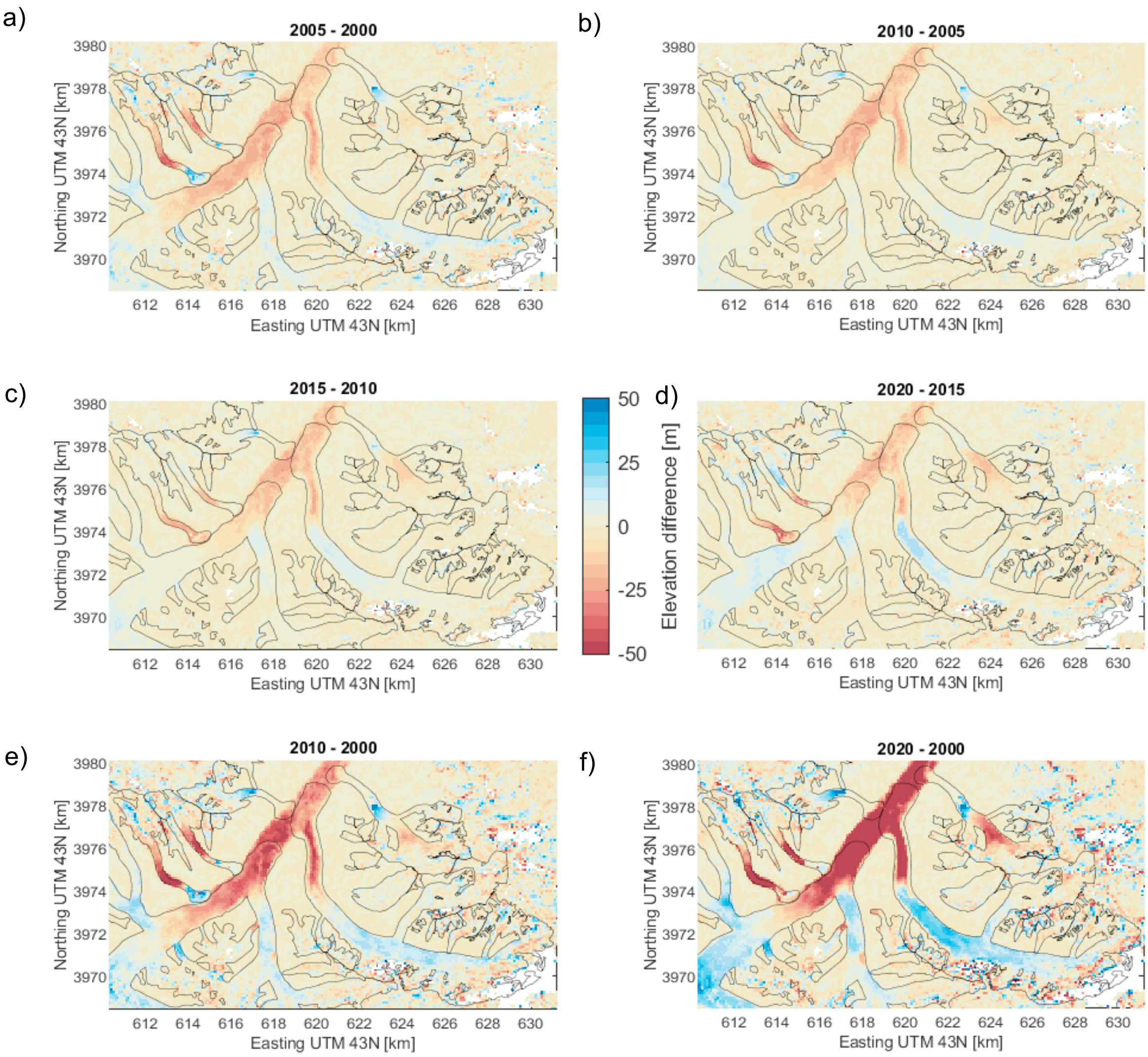

Fig. S13: DEM differences over four periods from Hugonnet et al. 2021. a) 2000-2004, b) 2005-2009, c) 2010-2014, d) 2015-2019, e) 2010-2000, f) 2020-2000.

Supplemental animations

Time series from Sentinel-1

Radar satellites can 'see' through clouds and Sentinel-1 offers frequent and systematic coverage in areas prone to monsoon clouds as the Himalayas. Despite radar speckle and 74 m x 56 m spatial resolution of 20x4 multi-looked products, the rapid advance of Chongtar glacier since July 2020 can be clearly observed in Sentinel-1 backscattering intensity images (Figure SA). Changes in backscattering intensity at the glacier surface are mostly due to a change in the physical properties of the ice, e.g. liquid water resulting from melting reduces intensity considerably. The animation of 12-days Sentinel-1 backscattering intensity images shows the sudden advance of South Chongtar glacier in Summer 2020. The file is named 'chongtar_surge_anim.gif'.

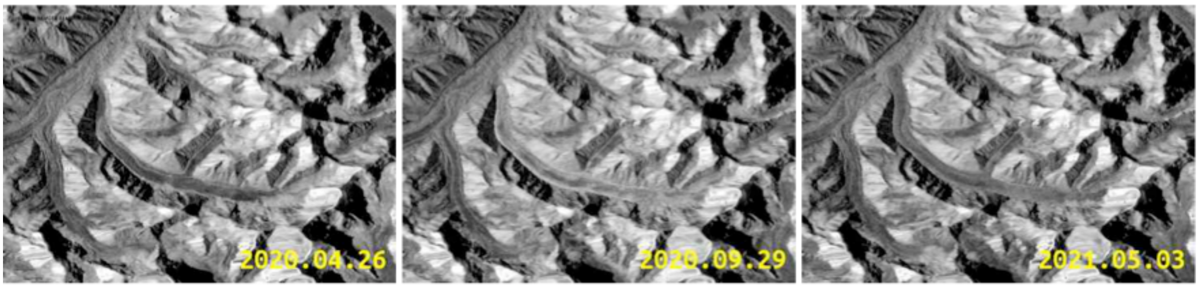

Figure SA: Sentinel-1 multi-looked backscattering intensity images of South Chongtar Glacier for (a) 26.4.2020, (b) 29.9.2020 and (c) 3.5.2021. The time series and the image extracts shown above contain modified Copernicus Sentinel-1 data 2020/21.